Direct CO_2 Reduction to CO with an Fe_4S_4-Based Coordination Polymer

Linh N. V. Le,[1†] Andrea Darù,[1†] Špela Kunstelj,[1] Anna Wuttig,[1] Laura Gagliardi,[1,2] and John S. Anderson[1*]

[1]Department of Chemistry, University of Chicago, Chicago, IL 60637, United States
[2]Pritzker School of Molecular Engineering, University of Chicago, Chicago, IL 60637, United States
[†]Equal contribution
Supporting Information Placeholder

ABSTRACT: Fe_4S_4 clusters play essential roles in nature, classically in electron transport but increasingly in newly discovered reactivity or catalysis. These roles have spurred interest in developing synthetic Fe_4S_4 systems and while several molecular and material systems built from Fe_4S_4 clusters have been developed, comparatively few examples of synthetic Fe_4S_4 cluster-based catalysts exist. Herein, we present the use of an Fe_4S_4-based coordination polymer as a catalyst for the direct and selective electroreduction of CO_2 to CO. Computational studies suggest that the reaction proceeds through CO_2 binding to a reduced Fe_4S_4 cluster, followed by a series of protonation, reduction, and H_2O loss steps to yield a CO-bound cluster that can finally exchange with CO_2 to restart the catalytic cycle. CO bound clusters are predicted to be thermodynamically stable, suggesting that carbonyl species might be off-cycle intermediates. Mechanistic CV studies as well as *in situ* studies by IR spectroscopy provide evidence for carbonyl-ligated clusters, supporting these compounds as unusual examples of small molecule binding to Fe_4S_4 clusters. This work establishes Fe_4S_4 cluster-based coordination polymers as direct electrocatalysts for CO_2 reduction and provides mechanistic insights into how these species mediate catalytic conversions of small molecules.

INTRODUCTION

Iron-sulfur clusters are among the most classic metallocofactor motifs, with functions including electron transport, catalysis, sensing, and even gene expression.[1–4] These species possess a variety of structures, ranging from Fe_2S_2 rhombs and Fe_4S_4 cubanes to more bespoke clusters with complex architectures like the FeMo cofactor in nitrogenase.[3] While the Fe_4S_4 form most commonly participates in electron transfer enabled by mixed-valency and facile switching between +2 and +3 oxidation states at Fe,[5–7] there is increasing evidence that these cuboidal clusters can serve as reactive centers or catalysts. For example, Fe_4S_4 clusters in radical SAM enzymes catalyze the formation of the reactive 5'-dAdo radical through an organometallic intermediate, Ω, involving an alkyl deoxyadenosyl group bound to an Fe vertex through the 5'-carbon atom.[8,9] Likewise, the aconitase enzyme contains a Fe_4S_4 unit with a solvent-bound Fe site involved in the catalytic isomerization of citrate to isocitrate.[10–12] These and other emerging findings motivate efforts to use these motifs as catalytic centers in synthetic systems as well.

Towards this end, a limited but increasing number of synthetic Fe_4S_4 systems have been investigated as catalysts (Figure 1).[13–16] A soluble $Fe_4S_4Cl_4^{2-}$ cluster was used as a catalyst for the hydrogenation of stilbene or diphenylacetylene to 1,2-diphenylethane, but requires stoichiometric amounts of highly reactive PhLi as an additive.[13] Other soluble $Fe_4S_4(SR)_4^{2-}$ clusters mediate the reduction of CO_2 in dimethylformamide (DMF) to oxalate, formate, and trace CO under electrochemical conditions,[14] or to CH_4 and C_{2+} hydrocarbons with SmI_2 as a chemical reductant (Figure 1A and B respectively).[15] While these are important advances, these examples all feature only moderate selectivity with at least three products formed. Furthermore, these studies provide little mechanistic insight, with no spectroscopic data on possible intermediates. In parallel, model chemistry involving small molecule substrate binding to Fe_4S_4 clusters remains rare, with only a few reported examples of CO,[17,18] NO,[19,20] isocyanide,[21,22] and alkene/alkyne[23] binding reported so far. Hence, an in-depth study of Fe_4S_4-cluster mediated catalytic systems can shed light on new reactivity patterns for these motifs.

Our laboratory recently built upon work by Dey *et. al.* using $Fe_4S_4(SPh)_4^{2-}$ as a concerted proton-electron transfer (CPET) mediator in conjunction with the cocatalyst $Mn(bpy)(CO)_3Br$ in acetonitrile (MeCN) for the electrochemical reduction of CO_2 to formic acid.[24] We previously rationalized that heterogenization of Fe_4S_4 clusters might enhance catalysis and enable recyclability, and so we employed the coordination polymer (CP) $[Fe_4S_4(BDT)_2][NMe_4]_2$ (**1-NMe$_4$**, BDT = 1,4,-benzenedithiol) in a similar manner with $Mn(bpy)(CO)_3Br$ to yield formic acid with good Faradaic efficiencies (FEs, Figure 1C).[25] Furthermore, heterogenization enabled additional mechanistic insights with *in situ* surface enhanced IR absorption spectroscopy (SEIRAS) in an attenuated reflectance mode, supporting that heterogenization can also be useful for structural characterization of the electrified interface. However, given the prior examples of homogeneous Fe_4S_4 systems serving as *direct* catalysts with no added co-catalyst (Figure 1A,B), as well as the increasing evidence for small-molecule binding and conversion at these sites, we wanted to examine the electrocatalytic activity of these CP systems without added Mn species.

Here, we demonstrate that Fe_4S_4-based CPs can directly serve as electrocatalysts for the reduction of CO_2. Controlled potential electrolyses produce the C_1 feedstock CO with up to 80% FE (Figure 1).[26] More importantly, heterogenization again provides mechanistic insight, and combined electrochemical,

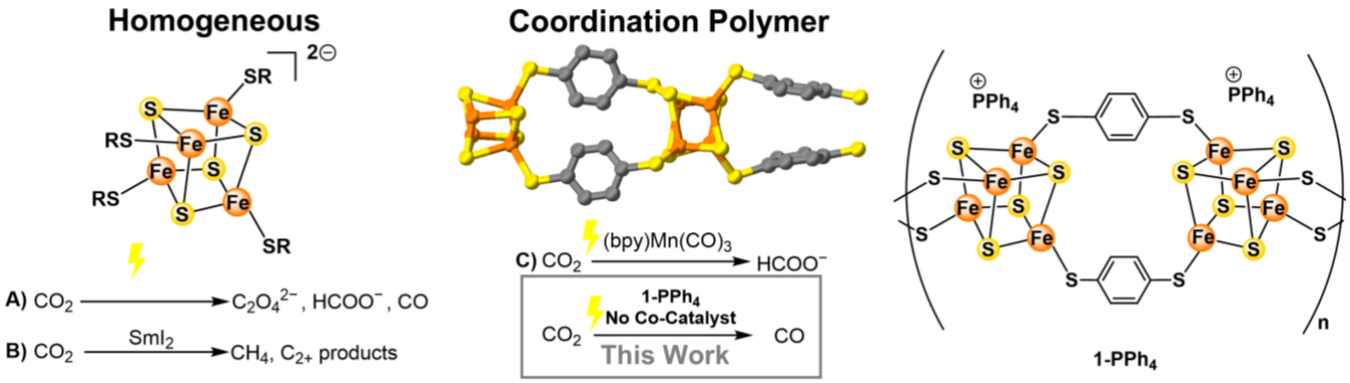

Figure 1. Left: Catalysis with homogeneous Fe_4S_4 clusters (ref. 14-15), showing product mixtures from CO_2 reduction. Center: Catalysis with heterogeneous Fe_4S_4-based coordination polymers (CPs), with a previous example of CO_2 reduction to formate in the presence of (bpy)$Mn(CO)_3$ cocatalyst (ref. 25), and this work on selective CO_2 reduction to CO without the need for an added cocatalyst. Right: Structure of **1-PPh_4**.

computational, and spectroscopic data support small molecule binding to the Fe_4S_4 clusters. Specifically, we find evidence for a CO-bound cluster intermediate, providing a rare example of small molecule binding on a catalytically active Fe_4S_4 system. These findings add to the growing body of literature on how Fe_4S_4 clusters can serve as reactive centers, and they provide important spectroscopic references for bound small molecules.

RESULTS AND DISCUSSION

Electrocatalytic Reduction of CO_2 to CO

Well-defined examples where Fe_4S_4 clusters can serve as direct catalysts for small molecule conversion are very limited, and so we turned to investigating the viability of these moieties in CO_2 reduction. We initially tested an Fe_4S_4-based CP for electrocatalysis with 2,2,2-trifluoroethanol (TFE) and/or CO_2 in dry MeCN by cyclic voltammetry (CV). We opted for the recently reported CP $[(Fe_4S_4)(BDT)_2][[PPh_4]_2$ (**1-PPh_4**, Figure 1) instead of the previously used **1-NMe_4** analog because of a higher degree of crystallinity and yield.[27]

1-PPh_4 was dropcast onto a glassy carbon electrode as a suspension in DMF with poly(vinylidene fluoride) (PVDF) as a binder for adhesion to the electrode surface. With only **1-PPh_4** present, the CV shows a broad quasi-reversible feature at ~−1.5 V (all potential values quoted vs. Ag^+/Ag) assigned to the $[Fe_4S_4]^{2+}/[Fe_4S_4]^+$ couple consistent with the previously reported **1-NMe_4**,[25,28] and a prominent irreversible reduction at ~−2.2 V (Figure S5). This feature is not present in **1-NMe_4**,[28] but is also observed in the soluble compound **$(PPh_4)_2Fe_4S_4(SPh)_4$**, which plausibly arises from the reduction of PPh_4^+.[29] We propose that this prominent peak in **1-PPh_4** may overlap with the $[Fe_4S_4]^+/[Fe_4S_4]^0$ redox couple, expected to be at around −2.2 V. In addition, no notable catalytic features appeared when scanned cathodically (Figure 2, dashed).

When the electrolyte solution in dry MeCN was sparged with CO_2 for 20 minutes, the CV shows a slight catalytic feature with an onset potential of about −2.0 V (Figure 2, red). While we note that the irreversible wave at −2.2 V persists in the presence of CO_2, the increased reductive current compared to that observed in its absence suggests electrocatalytic activity towards CO_2 reduction. As no proton source is provided, CO_2 reduction can proceed with trace water as commonly observed in hygroscopic solvents such as MeCN or through the simple coupling of $CO_2^{\bullet-}$ radicals.[30,31] When only TFE was added, an enhanced reductive feature appeared beginning at −2.4 V, assigned to the hydrogen evolution reaction (HER) (Figure 2, blue). In contrast, when both CO_2 and TFE were present, a suppression of the more cathodic HER feature was observed,

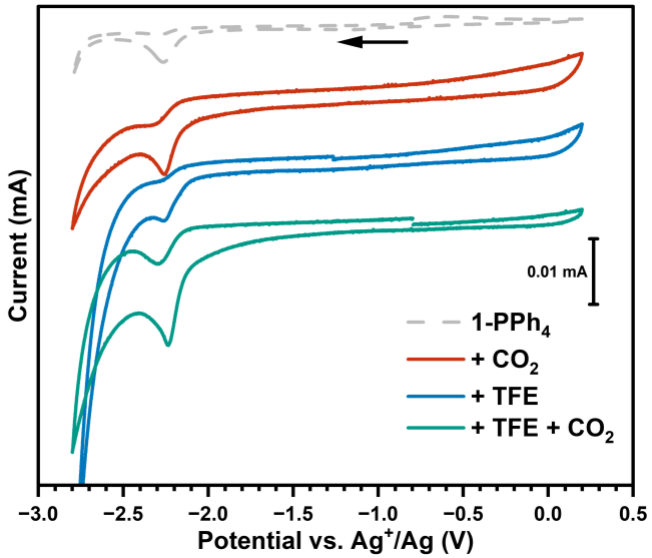

Figure 2. CVs of **1-PPh_4** (with PVDF binder on glassy carbon disk electrode) only, in the presence of CO_2, TFE, and both CO_2 and TFE. Conditions: 0.1 M $TBAPF_6$ in MeCN as electrolyte, 0.2 M TFE (if present), 20 minutes CO_2 sparging (if present), 100 mV s^{-1} scan rate.

with an enhancement of a catalytic wave starting at ~−1.7 V and a peak current at ~−2.2 V, which we assign to CO_2 reduction (Figure 2, teal). We note that mediated outer-sphere reduction of CO_2 is documented. Enhanced current density at −2.2 V is also observed in the absence of CO_2 (Figure 2, dashed). This again may arise from PPh_4^+ reduction,[29] but further increases in the presence of CO_2 may be facilitated via an outer-sphere electron transfer pathway from the reduced species.[32]

Encouraged by these results, we performed controlled potential electrolyses (CPE) on the same reaction mixture at −2.3 V. After 1 h, the headspace was sampled and analyzed by gas chromatography (Figure S1), which revealed the formation of CO and H_2 with FEs of 79% and 19% respectively, accounting for a total FE of 98% with a turnover frequency (TOF) of 61 h^{-1} for CO (calculated from the number of moles of CO produced per mol of cluster used). The ~80:20 ratio of CO:H_2 resembles that of synthesis gas (syngas) used in bioreactors for fermentation to higher molecular weight products such as ethanol.[33] The suppressed HER with **1-PPh_4** also raises the possibility of reducing other small organic substrates, an area

Table 1. Comparison of H_2 and CO yields under different reaction conditions (averages and standard deviations in parentheses are derived from duplicates).

Conditions	FE(H_2)	FE(CO)	FE(total)	CO:H_2
standard†	19(1)	79(7)	98(8)	4.3(0.1)
−2.0 V	2(1)	4(1)	5(1)	1.8(0.8)
−2.5 V	62(10)	46(15)	108(10)	0.7(0.3)
only PVDF no cluster	19(10)	24(5)	43(15)	1.3(0.5)
THF solvent	trace	trace	-	-
no TFE	0	2(1)	2(1)	-
0.2 M NEt_3HBF_4 as acid	104(5)	0	104(5)	0
0.2 M H_2O as acid	6(2)	4(2)	9(2)	0.7(0.2)
1-NMe$_4$	3(1)	15(4)	18(6)	4.9(0.9)
(PPh$_4$)$_2$Fe$_4$S$_4$(SPh)$_4$ 2 mM	48(3)	8(7)	57(4)	0.2(0.2)

†Standard conditions: 0.1 M $TBAPF_6$ in MeCN as electrolyte, 0.2 M TFE, 20 minutes CO_2 sparging, −2.3 V vs. Ag^+/Ag for 60 minutes.

which we are interested in investigating. Formic acid was not observed by ^{1}H NMR spectroscopy of the MeCN solution with any appreciable yield (Figure S2). X-ray photoelectron spectra (XPS) of the electrocatalytic films before and after the reaction are similar in both the Fe 2p and S 2p regions, supporting intact clusters during and after catalysis (Figure S11). This is also corroborated by grazing incidence X-ray diffraction (GIXRD) (Figure S12) and inductively-coupled plasma – optical emission spectroscopy (ICP-OES) (Table S2) conducted on the film before and after the reaction, showing the retention of the $Fe_4S_4(BDT)_2$ chains, albeit with some cation exchange between PPh_4^+ and NBu_4^+ (TBA) from the electrolyte. Finally, UV-vis analysis of electrolyte solutions before and after soaking with **1-PPh$_4$** electrodes suggest there is no catalyst leaching into solution (Figure S13).

We then explored other reaction conditions to understand how different factors affect the gaseous product compositions and yields (Table 1). Under a slightly more positive applied potential of −2.0 V, low currents and yields were observed, consistent with our previous report where only small amounts of products were formed with **1-NMe$_4$** at similar potentials.[25] Enhanced current is observed at a more negative potential of −2.5 V, but this is largely due to increased HER at these potentials resulting in a lower FE for CO. A control experiment with only the PVDF binder on a glassy carbon electrode resulted in low FEs and selectivity for CO, suggesting that **1-PPh$_4$** is necessary for selective CO formation. In addition, the solvent choice is critical to the reaction, as less polar solvents like THF lead to lower currents and yields.[34,35]

Consistent with the CV results, the addition of acid is required for the formation of CO. Moreover, the pK_a of the acid also dictates the efficiency of the transformation. The reaction requires a sufficiently strong acid to protonate CO_2 reduction intermediates, but not acidic enough to favor HER, with TFE (pK_a = 23.6 in DMSO)[36] lying within the appropriate range. Consequently, $[HNEt_3][BF_4]$ (pK_a = 9.0 in DMSO)[37] led to solely HER, while water (pK_a = 31.4 in DMSO)[38] resulted in low currents and little CO formation.

In comparison, replacing **1-PPh$_4$** with **1-NMe$_4$** leads to a similar CO:H_2 ratio of ~4:1, although with dramatically lower FE and activity (Table 1). This suggests that the preference for CO formation over H_2 is intrinsic to the $Fe_4S_4(BDT)_2$ polymer chains, while the electrocatalytic activity is tuned by the countercation. We hypothesize that the larger PPh_4^+ cation allows for greater chain-to-chain separation, providing more space for CO_2 binding and protonation by nearby TFE molecules. In addition, the phenyl rings on PPh_4^+ may also improve electron transfer from the electrode to the Fe_4S_4 clusters compared to the methyl groups on NMe_4^+.

Several observations support this hypothesis. The homogeneous reaction catalyzed by the soluble cluster **(PPh$_4$)$_2$Fe$_4$S$_4$(SPh)$_4$** leads to primarily H_2. This is plausibly due to the ease of H_2 formation from encounter between two protonated clusters in solution, while in **1-PPh$_4$** the protonated sites are immobilized in the polymer chain preventing combination to form H_2. Furthermore, the different CO:H_2 ratios for **1-PPh$_4$** and **(PPh$_4$)$_2$Fe$_4$S$_4$(SPh)$_4$** exclude any central role for PPh_4^+ as the main CO_2 reduction catalyst. Thus, the selectivity for CO vs. H_2 is primarily conferred by the heterogenization of Fe_4S_4 clusters into a CP, while the PPh_4^+ cations more likely play a role in facilitating substrate or electron transfer.

Computational Modeling

To gain insights into the reaction mechanism leading to the conversion of CO_2 to CO, including intermediate complexes and competitive reaction steps, we employed computational modeling based on density functional theory (DFT) with the TPSSh functional (see Supporting Information).[39,40] The primary reaction mechanism is presented in Scheme 1, with secondary pathways discussed in the Supporting Information (Schemes S1 and S2). The applied potential for the reduction steps was incorporated by calculating the energy of one electron at the experimental applied potential of −2.3 V using Faraday's law (see Supporting Information).

At this negative potential, the direct reduction of CO_2 to its radical anion is feasible,[41] as well as the reduction of Fe(III) to Fe(II) and potentially even to Fe(I) in iron-sulfide systems,[42–44] especially in the presence of highly π-accepting ligands like CO that can stabilize electron-rich Fe(I) centers.[17,45,46] Our computations suggest that these highly reduced forms of Fe_4S_4-clusters are energetically accessible and that they may therefore be viable intermediates in catalysis.

We considered two primary mechanistic pathways featuring either thiolate protonation as previously proposed (Scheme 1A)[25] or reduction to an all-ferrous cluster and direct CO_2 binding (Scheme 1B). Both pathways are energetically viable and the addition of more electrons to generate more reduced species for both pathways is calculated to be favorable (Schemes S1 and S2). For thiolate protonation, reduction and protonation of **1** to form **1H** is quite exergonic (–83.7 kcal/mol), but subsequent CO_2 binding to form **1H-CO$_2$** is uphill. Tautomerization to form **1-CO$_2$H** is again exergonic, down to –85.9 kcal/mol from **1**, and subsequent protonation and reduction to release H_2O is very favorable, as expected. We note that the metallocarboxylic acid intermediates exhibit the greatest structural deformation among the series, with cleavage of one Fe-sulfide bond.

In comparison, the computed mechanism involving direct reduction and CO_2 binding requires reduction to at least an all-ferrous species (**2**). Interestingly, calculations suggest that CO_2 binding to **1** and to a singly reduced $Fe^{III}Fe^{II}_3$ cluster is unfavorable, whereas binding to **2** (Fe^{II}_4) becomes slightly exergonic (–2.0 kcal/mol). Further reduction makes CO_2 binding increasingly exergonic.

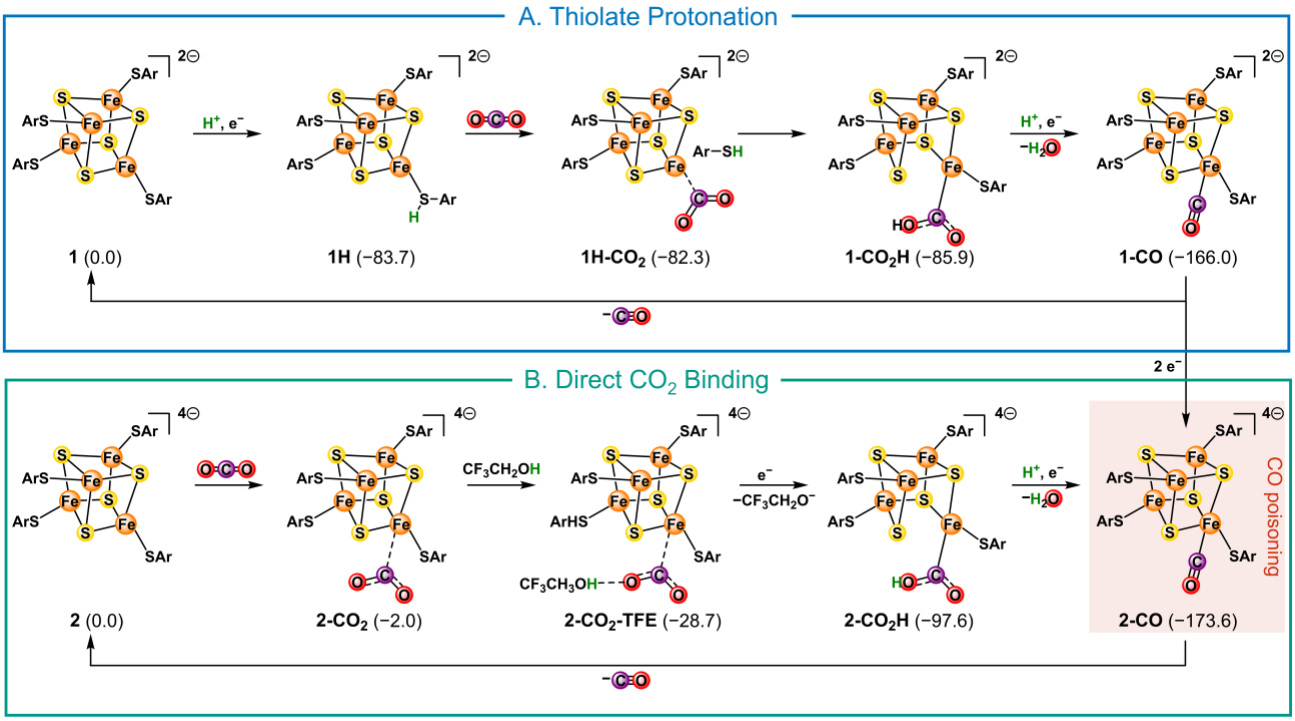

Scheme 1. Computed reaction mechanisms for A: thiolate protonation and B: reduction and direct CO_2 binding. Each pathway is referenced independently to the starting species. For simplicity in calculations, the Ar group is modeled as phenyl, and the counterion is PMe_4 instead of PPh_4. Free energies are in kcal/mol (T = 298 K) and are calculated at the DFT level, considering all species solvated with MeCN solvent (see Computational Details).

The next modelled step involves favorable TFE association before a very exergonic first hydrogen-atom transfer (HAT) from TFE to the bound CO_2 species, generating **2-CO$_2$H** at –97.6 kcal/mol. As mentioned, **2-CO$_2$H** exhibits significant structural deformation among the computed intermediates: the Fe—S bond adjacent to the CO_2-bound Fe center elongates from 2.4 Å to 3.7 Å. Subsequently, a second HAT step converts the *CO(OH) fragment to CO, releasing H_2O and restoring the previously broken Fe—S bond to form **2-CO** (overall ΔG = −173.6 kcal/mol). Both pathways require the release of CO to re-enter the catalytic cycle. Our calculations also show that CO and CO_2 coordination are similar in free energy (Scheme S1), but reduction of these CO-bound species is calculated to be quite favorable (**4-CO** and **4H-CO**, Scheme S1). This suggests that CO may act as an inhibitor by competitively binding to the cluster and blocking CO_2 coordination. This computational prediction is validated with experimental tests to examine possible CO poisoning as described below.

Related computational studies were previously reported by Hu and coworkers.[15] However, there are several key differences between the present system and their earlier study. Firstly, a chemical reductant (SmI_2) was used in the previous work. We also do not observe any C–C coupling activity in our system. This can likely be explained by the proposed mechanism from the prior report, wherein the authors invoke the dissociation of one Fe-thiolate bond for C–C coupling to occur through carbonyl-bound intermediates. In **1-PPh$_4$**, the thiolate linkers are flanked between two Fe_4S_4 units and are therefore difficult to completely dissociate from the Fe sites in the solid state. Experimental attempts at reductions under CO or to generate open Fe centers by methylating the thiolate sulfurs of **1-PPh$_4$** with MeOTf or MeI did not lead to any observable C–C bond formation. Although our computations indicate that protonation of the linker and CO or CO_2 coordination might promote Fe–thiolate dissociation, we hypothesize that these dissociated species are short-lived in a polymeric material, leading to much faster linker coordination than C–C bond formation.

Mechanistic Tests of CO Binding

Based on the calculated mechanism shown in Scheme 1, a CO-bound species might be involved in the reaction as a resting state. In addition, calculations also suggest that CO might act as a catalyst poison as is commonly observed in CO_2 reduction electrocatalysis.[47–51] Thus, we conducted different experiments to understand how CO interacts with our cluster system.

We collected CV data of **1-PPh$_4$** in an atmosphere of CO_2 with added CO in similar amounts as are produced during electrolyses (50 to 300 µL in a 20 mL headspace, Figure 3A and B). As CO is added, a small CV feature appears at −2.17 V which merges with the larger feature at higher CO concentrations causing an overall shift of the peak current from ~−2.25 to ~−2.22 V (Figure S8). We hypothesize that this feature might arise due to the binding of CO to the cluster. In support of this hypothesis, this feature increases in intensity with higher CO concentrations to form a shoulder and eventually a broader overall wave around −2.2 V. While still broad, differential pulse voltammetry (DPV) supports the presence of these two features (Figure S9). The broadness of these features can likely be attributed to several different possible redox reactions present under equilibrium exchange conditions including with CO- or CO_2-bound species as well as unbound clusters. In addition, the reductive adsorption of CO could be facilitated by the removal of adsorbed anions, as charge transfer is not expected for neutral adsorbates.[52]

In terms of catalysis, the current at the electrolysis potential of −2.3 V decreases with small quantities of added CO

comparable to the amounts typically produced in reactions and consistent with some degree of catalyst deactivation by CO (Figure 3C). When the atmosphere is replenished with CO_2 by sparging for 20 minutes to purge out the CO, the CV becomes identical to before adding CO (Figure 3A) and the current is restored (Figure 3C, red point), suggesting that CO binding and poisoning is reversible. These observations suggest that CO release is rate-limiting as predicted computationally, and that CO-bound species may be long-lived enough to observe by spectroscopic methods.

Spectroscopic Studies of CO Binding

The detection of a CO-bound Fe_4S_4 cluster species is of significant interest, as observation of small molecule binding on iron-sulfur clusters is rare generally. Very few examples of both synthetic and biological iron-sulfur clusters with terminally bound CO ligands have been reported.[17,18,45,53,54] In an attempt to spectroscopically observe CO binding, we exposed **1-PPh$_4$** to 1 atm CO with or without TFE as the acid source and a reductant like $KC_{10}H_8$. ATR-IR spectroscopy reveals no change to the material with added CO and TFE, but a small feature at 1900 cm^{-1} appears in the presence of CO and $KC_{10}H_8$ (Figures S14 – S15). This lies within the range for CO-bound iron-sulfur clusters,[17,18,45,55] suggesting that CO binding only occurs under reduction of the cluster, similarly to nitrogenase and other species.[17,53,54] The low intensity of the feature can be attributed to the inefficiency of reduction and CO binding using a chemical reductant.

Motivated by this, we performed CV-coupled SEIRAS on a film of **1-PPh$_4$** with PVDF as the binder deposited on an Au-coated Si prism in a CO-saturated MeCN solution to subject the cluster to a constant reductive environment that can increase the degree of CO coordination. CO gas was introduced by continuously bubbling CO through the MeCN solution until saturated for about 3 minutes (details in Supporting Information). Under these conditions, we observe a broad new feature starting at 1970 cm^{-1} that sharpens and Stark shifts to ~1900 cm^{-1} when scanned to more negative potentials (Figure 4 and Table S3). Notably, the background with only PVDF does not show this feature under CO (Figure S28). This suggests a changing CO environment in the presence of the cluster, consistent with CO binding as suggested by computation. We list below some support for this possible scenario.

The features at 1900 cm^{-1} only appear when the system is under CO with a negatively applied potential of at least −2.2 V, near the major features we observe by CV. This is confirmed computationally via DFT modeling, where such binding is favorable only after **1** undergoes at least two reduction steps (Scheme S1). Furthermore, these features lie in a comparable region to other CO-bound iron-sulfur clusters.[17,18,45,55] The peaks decrease in intensity at more positive potentials suggesting fewer bound CO molecules, consistent with the lower electron density in the cluster, decreasing the level of π-backbonding to CO to weaken Fe–C bonds for CO release. This provides support for the reversible interaction between the cluster and CO, consistent with the CV data in Figure 3 and the computational results.

Indeed, we note that the SEIRAS features around 1900 cm^{-1} are not observed for experiments conducted in the absence of CO (Figures S18 – S19) nor when CO and **1-PPh$_4$** are absent (Figures S26 – S27), consistent with the assignment of this feature to the presence of CO at the electrified interface. In addition, we do not observe any features in this region when experiments are conducted in the presence of CO but without **1-PPh$_4$** (Figures S28 – S29), confirming the absence of any exposed Au surface that can bind CO terminally, which typically appears at 2100 cm^{-1},[56,57] and can shift to ~1982 cm^{-1} under a similar reductive potential bias.[58,59]

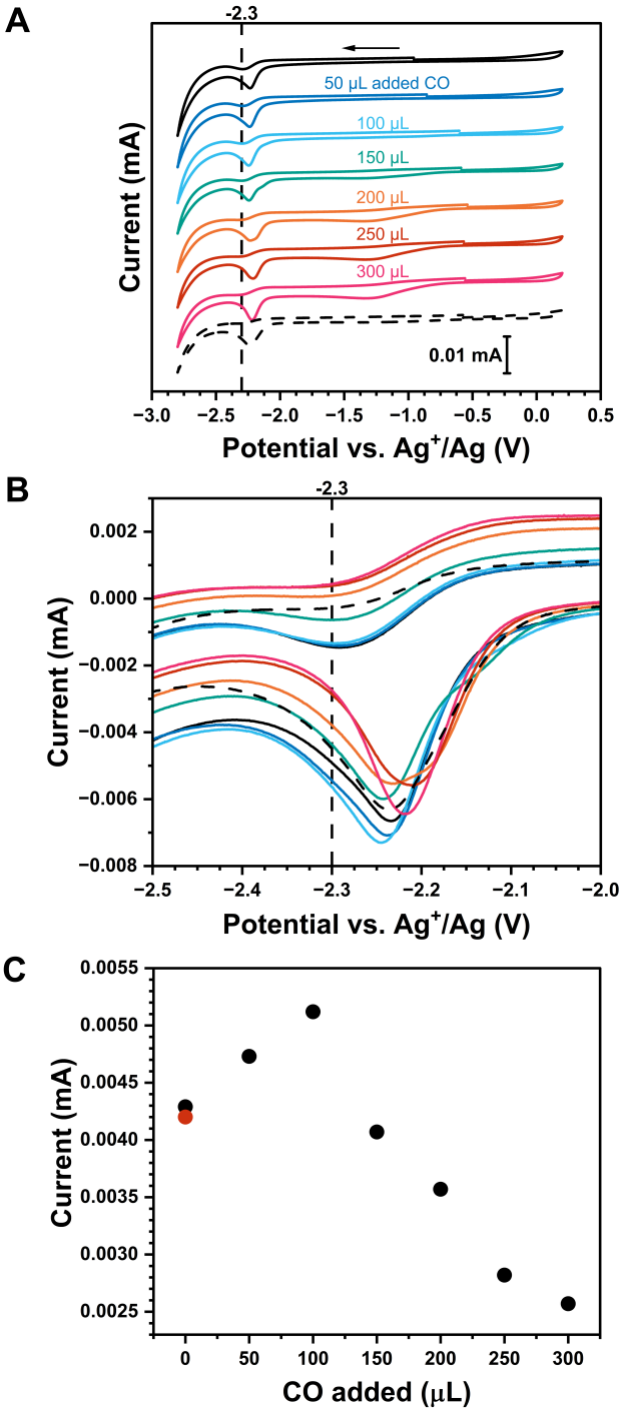

Figure 3. A) CVs of **1-PPh$_4$** (with PVDF binder on glassy carbon disk electrode) in the presence of 0.2 M TFE, CO_2, and variable amounts of added CO. Conditions: 0.1 M $TBAPF_6$/MeCN electrolyte, 20 minutes CO_2 sparging before adding CO, 100 mV s^{-1} scan rate. The dashed line shows the CV after sparging with CO_2 again for 20 minutes to remove CO. B) Zoomed-in view of the CVs around −2.2 V where the currents in the region from −1.5 to −2.0 V are overlapped to account for differences in the background current. The dashed line shows the CV after sparging with CO_2 again for 20 minutes to remove CO. C) Plot of the current at −2.3 V vs. amount of CO added, with the current after purging the system with CO_2 for 20 minutes in red.

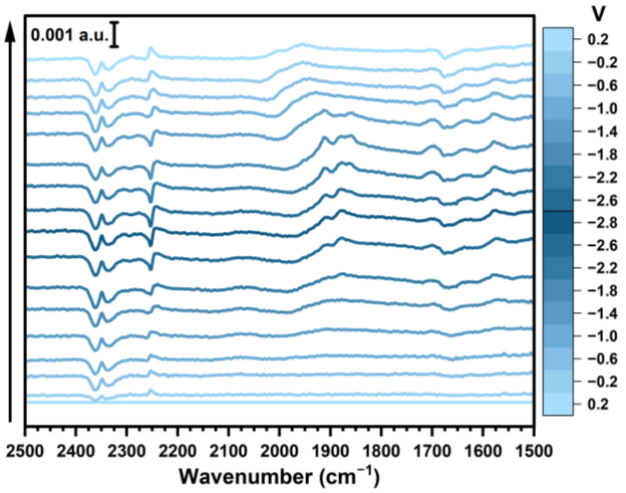

Figure 4. SEIRAS of **1-PPh$_4$** (with PVDF binder) on Au surface under CV from 0.2 V to −2.8 V then back to 0.2 V after purging with CO until saturation for 3 minutes. In all SEIRAS experiments, 0.2 M TFE and 0.1 M TBAPF$_6$ in MeCN were used, with CVs from 0.2 to −2.8 V at a 2 mV s^{-1} scan rate. The bulk CO was subtracted by using a background spectrum with purged CO.

The computationally predicted C–O stretching vibrations agree well with the features observed in SEIRAS and ATR-IR spectra, with a value of 2033 cm^{-1} predicted for unreduced **1-CO**, which decreases with every reduction to 2013 cm^{-1}, 1967 cm^{-1} (for **2-CO**), 1884 cm^{-1}, and eventually 1812 cm^{-1}. Similar vibrational frequencies are found for species with protonated thiolates with CO vibrational modes between 1800 and 1900 cm^{-1} (Scheme S2). These values are consistent with the experimental data and also provide a plausible explanation for the broadness of the SEIRAS feature, likely arising from multiple species with similar vibrational frequencies. We tentatively assign the two sharp peaks observed experimentally to **2-CO** and **3-CO** (Scheme S1). Most interestingly, these signals suggest that SEIRAS allows for the observation of electrochemically generated CO-bound species relevant to the catalytic reduction of CO_2 to CO. We note that we observe a broad feature at ~1900 cm^{-1} for experiments conducted on films of **1-PPh$_4$** in the presence of CO_2 without exogenously added CO (Figures S22 – S23) which does not appear under only N_2 (Figures S18 – S19) in agreement with the experimental observation of CO as the primary product of CO_2 reduction with the heterogenized **1-PPh$_4$**. This lower intensity of this feature is consistent with the transient role of CO-bound species as intermediates in the reaction, which should not accumulate in large quantities under the catalytic conditions with excess CO_2. We note the emergence of the broad feature at ~1900 cm^{-1} in Figure S23 at −1.8 V, in line with the onset of considerable reductive current observed in the presence of TFE and CO_2 in Figure 2.

Similarly, recent work from the DeBeer group on nitrogenase under a CO atmosphere utilizing SEIRAS assigns a peak at 1970 cm^{-1} under reductive conditions to a terminally bound CO on FeMoco.[60] This peak also exhibits a Stark shift where it moves to lower wavenumbers at more negative potentials, arising from the increase in the electron density in the cluster and more π backbonding to the terminal CO ligand. In that work, the authors propose that the breadth of this feature might arise from multiple CO-bound species. They also observed a small feature at 2600 cm^{-1} that shifts upon deuteration, assigned to an S–H bond. We did not observe such a corresponding feature in our experimental data (Figure S20), although our computational results suggest that an intermediate with a protonated sulfur atom is possible, with a predicted S–H stretching frequency of ~2300 cm^{-1}. As previously noted, these S–H bands are usually difficult to observe by IR spectroscopy because of their low intensity and broadness,[60–62] so other techniques should be employed to definitively confirm this possibility.

Interestingly, we observe up to three sharp features superimposed on a broad envelope in the region assigned to CO-bound species. The observation of multiple features in this region may suggest the presence of multiple different carbonyl containing species, as proposed by DeBeer and coworkers in SEIRAS studies on FeMoco.[60] The Stark shift convolutes any comparison of these features with predictions from theory, but we postulate that these species could correspond to different carbonylated cluster redox isomers, clusters with multiple bound CO ligands, or carbonylated clusters with combinations of different protonation or redox states (such as those identified in Scheme S2). Regardless of their exact assignment, the presence of multiple features supports a complex speciation under electrochemical bias.

CONCLUSION

In this work, we have demonstrated the ability of the Fe_4S_4 CP **1-PPh$_4$** to catalyze the reduction of CO_2 to CO and H_2 in a heterogeneous reaction. The catalyst has a preference for CO production over H_2, highlighting its ability to suppress HER. This suggests the possibility of using the material for H-atom transfer to other substrates as well. Notably, while Fe_4S_4 clusters have been demonstrated as CPET mediators,[24,25] this report shows that they can also serve as direct catalysts (without any co-catalyst) when heterogenized into a coordination polymer.

The stability imparted by the polymer also allows for spectroscopic studies to observe transient substrate-bound species. Computational studies propose that the reaction proceeds through a CO-bound intermediate, the evidence for which is suggested by *in situ* SEIRAS. This provides unusual spectroscopic support for gas binding to these clusters, as well as a framework to understand the use of synthetic iron-sulfur clusters as catalysts and to provide relevant mechanistic insights.

SUPPORTING INFORMATION

The Supporting Information is available free of charge at http://pubs.acs.org.

- xyz coordinates for computation
- Experimental section, additional characterization data, cyclic voltammetry, NMR spectra, computation details.

AUTHOR INFORMATION

Corresponding Authors

John S. Anderson - Department of Chemistry, University of Chicago, Chicago, IL 60637, United States; https://orcid.org/0000-0002-0730-3018; Email: jsanderson@uchicago.edu

Author Contributions

L.N.V.L. and A.D. contributed equally to this work.

Notes

The authors declare no competing interests.

ACKNOWLEDGMENT

This research was supported by the Catalyst Design for Decarbonization Center an Energy Frontier Research Center funded by the U.S. Department of Energy, Office of Science, Basic Energy Sciences under Award No. DE-SC0023383. We acknowledge the University of Chicago's Research Computing Center for providing the resources to carry out this work. L. N. V. L would like to thank the University of Chicago Material Research Center (MRSEC) for support through the Kadanoff-Rice Fellowship. We also thank Dr. Alexander Filatov for assistance with XPS data collection, and Ruiming Lin for help with ICP-OES.

REFERENCES

(1) Boncella, A. E.; Sabo, E. T.; Santore, R. M.; Carter, J.; Whalen, J.; Hudspeth, J. D.; Morrison, C. N. The Expanding Utility of Iron-Sulfur Clusters: Their Functional Roles in Biology, Synthetic Small Molecules, Maquettes and Artificial Proteins, Biomimetic Materials, and Therapeutic Strategies. *Coord. Chem. Rev.* **2022**, *453*, 214229. https://doi.org/10.1016/j.ccr.2021.214229.

(2) Johnson, D. C.; Dean, D. R.; Smith, A. D.; Johnson, M. K. Structure, Function, and Formation of Biological Iron-Sulfur Clusters. *Annu. Rev. Biochem.* **2005**, *74* (1), 247–281. https://doi.org/10.1146/annurev.biochem.74.082803.133518.

(3) Beinert, H.; Holm, R. H.; Münck, E. Iron-Sulfur Clusters: Nature's Modular, Multipurpose Structures. *Science* **1997**, *277* (5326), 653–659. https://doi.org/10.1126/science.277.5326.653.

(4) Waser, V.; Ward, T. R. Aqueous Stability and Redox Chemistry of Synthetic [Fe_4S_4] Clusters. *Coord. Chem. Rev.* **2023**, *495*, 215377. https://doi.org/10.1016/j.ccr.2023.215377.

(5) Lill, R. Function and Biogenesis of Iron–Sulphur Proteins. *Nature* **2009**, *460* (7257), 831–838. https://doi.org/10.1038/nature08301.

(6) Skeel, B. A.; Suess, D. L. M. Exploiting Molecular Symmetry to Quantitatively Map the Excited-State Landscape of Iron–Sulfur Clusters. *J. Am. Chem. Soc.* **2023**. https://doi.org/10.1021/jacs.3c02412.

(7) Wenke, B. B.; Spatzal, T.; Rees, D. C. Site-Specific Oxidation State Assignments of the Iron Atoms in the $[4Fe:4S]^{2+/1+/0}$ States of the Nitrogenase Fe-Protein. *Angew. Chem. Int. Ed.* **2019**, *58* (12), 3894–3897. https://doi.org/10.1002/anie.201813966.

(8) Byer, A. S.; Yang, H.; McDaniel, E. C.; Kathiresan, V.; Impano, S.; Pagnier, A.; Watts, H.; Denler, C.; Vagstad, A. L.; Piel, J.; Duschene, K. S.; Shepard, E. M.; Shields, T. P.; Scott, L. G.; Lilla, E. A.; Yokoyama, K.; Broderick, W. E.; Hoffman, B. M.; Broderick, J. B. Paradigm Shift for Radical S-Adenosyl-l-Methionine Reactions: The Organometallic Intermediate Ω Is Central to Catalysis. *J. Am. Chem. Soc.* **2018**, *140* (28), 8634–8638. https://doi.org/10.1021/jacs.8b04061.

(9) Horitani, M.; Shisler, K.; Broderick, W. E.; Hutcheson, R. U.; Duschene, K. S.; Marts, A. R.; Hoffman, B. M.; Broderick, J. B. Radical SAM Catalysis via an Organometallic Intermediate with an Fe–[5′-C]-Deoxyadenosyl Bond. *Science* **2016**, *352* (6287), 822. https://doi.org/10.1126/science.aaf5327.

(10) Castro, L.; Tórtora, V.; Mansilla, S.; Radi, R. Aconitases: Non-Redox Iron–Sulfur Proteins Sensitive to Reactive Species. *Acc. Chem. Res.* **2019**, *52* (9), 2609–2619. https://doi.org/10.1021/acs.accounts.9b00150.

(11) Weigel, J. A.; Holm, R. H. Intrinsic Binding Properties of a Differentiated Iron Subsite in Analogs of Native $[Fe_4S_4]^{2+}$ Clusters. *J. Am. Chem. Soc.* **1991**, *113* (11), 4184–4191. https://doi.org/10.1021/ja00011a020.

(12) Lloyd, S. J.; Lauble, H.; Prasad, G. S.; Stout, C. D. The Mechanism of Aconitase: 1.8 Å Resolution Crystal Structure of the S642A:Citrate Complex. *Protein Sci.* **1999**, *8* (12), 2655–2662. https://doi.org/10.1110/ps.8.12.2655.

(13) Inoue, H.; Suzuki, M. Catalytic Function of the Phenyl-Lithium-Treated $Fe_4S_4Cl_4^{2-}$ Cluster in the Hydrogenation of Cis- and Trans-Stilbenes. *J. Chem. Soc., Chem. Commun.* **1980**, No. 17, 817–818. https://doi.org/10.1039/C39800000817.

(14) Tezuka, M.; Yajima, T.; Tsuchiya, A.; Matsumoto, Y.; Uchida, Y.; Hidai, M. Electroreduction of Carbon Dioxide Catalyzed by Iron-Sulfur Cluster Compounds $[Fe_4S_4(SR)_4]^{2-}$. *J. Am. Chem. Soc.* **1982**, *104* (24), 6834–6836. https://doi.org/10.1021/ja00388a085.

(15) Stiebritz, M. T.; Hiller, C. J.; Sickerman, N. S.; Lee, C. C.; Tanifuji, K.; Ohki, Y.; Hu, Y. Ambient Conversion of CO_2 to Hydrocarbons by Biogenic and Synthetic [Fe_4S_4] Clusters. *Nat. Catal.* **2018**, *1* (6), 444–451. https://doi.org/10.1038/s41929-018-0079-4.

(16) Yuhas, B. D.; Prasittichai, C.; Hupp, J. T.; Kanatzidis, M. G. Enhanced Electrocatalytic Reduction of CO_2 with Ternary Ni-Fe_4S_4 and Co-Fe_4S_4-Based Biomimetic Chalcogels. *J. Am. Chem. Soc.* **2011**, *133* (40), 15854–15857. https://doi.org/10.1021/ja205981v.

(17) Brown, A. C.; Thompson, N. B.; Suess, D. L. M. Evidence for Low-Valent Electronic Configurations in Iron–Sulfur Clusters. *J. Am. Chem. Soc.* **2022**, *144* (20), 9066–9073. https://doi.org/10.1021/jacs.2c01872.

(18) Brown, A. C.; Suess, D. L. M. An Iron–Sulfur Cluster with a Highly Pyramidalized Three-Coordinate Iron Center and a Negligible Affinity for Dinitrogen. *J. Am. Chem. Soc.* **2023**, *145* (36), 20088–20096. https://doi.org/10.1021/jacs.3c07677.

(19) Kim, Y.; Sridharan, A.; Suess, D. L. M. The Elusive Mononitrosylated [Fe_4S_4] Cluster in Three Redox States. *Angew. Chem. Int. Ed.* **2022**, *61* (47), e202213032. https://doi.org/10.1002/anie.202213032.

(20) Bera, S.; Ghude, A.; Catalano, V. J.; Mouesca, J.-M.; García-Serres, R.; Murray, L. J. Nitrite Causes Nitrosative Stress to Iron Sulfur Clusters. *J. Am. Chem. Soc.* **2025**, *147* (26), 22329–22334. https://doi.org/10.1021/jacs.5c05636.

(21) Brown, A. C.; Suess, D. L. M. Controlling Substrate Binding to Fe_4S_4 Clusters through Remote Steric Effects. *Inorg. Chem.* **2019**, *58* (8), 5273–5280. https://doi.org/10.1021/acs.inorgchem.9b00360.

(22) Brown, A. C.; Thompson, N. B.; Suess, D. L. M. Activation of Strong π–Acids at $[Fe_4S_4]^+$ Clusters Enabled by a Noncanonical Electronic Structure. *J. Am. Chem. Soc.* **2024**. https://doi.org/10.1021/jacs.4c13490.

(23) Brown, A. C.; Suess, D. L. M. Valence Localization in Alkyne and Alkene Adducts of Synthetic $[Fe_4S_4]^+$ Clusters. *Inorg. Chem.* **2022**. https://doi.org/10.1021/acs.inorgchem.2c01353.

(24) Dey, S.; Masero, F.; Brack, E.; Fontecave, M.; Mougel, V. Electrocatalytic Metal Hydride Generation Using CPET

Mediators. *Nature* **2022**, *607* (7919), 499–506. https://doi.org/10.1038/s41586-022-04874-z.

(25) Jiang, N.; Darù, A.; Kunstelj, Š.; Vitillo, J. G.; Czaikowski, M. E.; Filatov, A. S.; Wuttig, A.; Gagliardi, L.; Anderson, J. S. Catalytic, Spectroscopic, and Theoretical Studies of Fe_4S_4-Based Coordination Polymers as Heterogenous Coupled Proton–Electron Transfer Mediators for Electrocatalysis. *J. Am. Chem. Soc.* **2024**, *146* (17), 12243–12252. https://doi.org/10.1021/jacs.4c03726.

(26) Ma, X.; Albertsma, J.; Gabriels, D.; Horst, R.; Polat, S.; Snoeks, C.; Kapteijn, F.; Eral, H. B.; Vermaas, D. A.; Mei, B.; Beer, S. de; Veen, M. A. van der. Carbon Monoxide Separation: Past, Present and Future. *Chem. Soc. Rev.* **2023**, *52* (11), 3741–3777. https://doi.org/10.1039/D3CS00147D.

(27) Mao, J.; Jiang, N.; Darù, A.; Filatov, A. S.; Burch, J. E.; Hofmann, J.; Vornholt, S. M.; Chapman, K. W.; Anderson, J. S.; Ferguson, A. L. Structure and Synthesizability of Iron–Sulfur Metal–Organic Frameworks. *J. Am. Chem. Soc.* **2025**, *147* (21), 17651–17667. https://doi.org/10.1021/jacs.4c16341.

(28) Horwitz, N. E.; Xie, J.; Filatov, A. S.; Papoular, R. J.; Shepard, W. E.; Zee, D. Z.; Grahn, M. P.; Gilder, C.; Anderson, J. S. Redox-Active 1D Coordination Polymers of Iron–Sulfur Clusters. *J. Am. Chem. Soc.* **2019**, *141* (9), 3940–3951. https://doi.org/10.1021/jacs.8b12339.

(29) Saveant, J. M.; Khac Binh, S. Electrochemical Reduction of Tetraphenylphosphonium Cation in Low Acidity Media. *Electrochim. Acta* **1975**, *20* (1), 21–26. https://doi.org/10.1016/0013-4686(75)85039-0.

(30) Kumar, A. S.; Pupo, M.; Petrov, K. V.; Ramdin, M.; van Ommen, J. R.; de Jong, W.; Kortlever, R. A Quantitative Analysis of Electrochemical CO_2 Reduction on Copper in Organic Amide and Nitrile-Based Electrolytes. *J. Phys. Chem. C* **2023**, *127* (27), 12857–12866. https://doi.org/10.1021/acs.jpcc.3c01955.

(31) König, M.; Vaes, J.; Klemm, E.; Pant, D. Solvents and Supporting Electrolytes in the Electrocatalytic Reduction of CO_2. *iScience* **2019**, *19*, 135–160. https://doi.org/10.1016/j.isci.2019.07.014.

(32) Gennaro, A.; Isse, A. A.; Savéant, J.-M.; Severin, M.-G.; Vianello, E. Homogeneous Electron Transfer Catalysis of the Electrochemical Reduction of Carbon Dioxide. Do Aromatic Anion Radicals React in an Outer-Sphere Manner? *J. Am. Chem. Soc.* **1996**, *118* (30), 7190–7196. https://doi.org/10.1021/ja960605o.

(33) Munasinghe, P. C.; Khanal, S. K. Biomass-Derived Syngas Fermentation into Biofuels: Opportunities and Challenges. *Bioresour. Technol.* **2010**, *101* (13), 5013–5022. https://doi.org/10.1016/j.biortech.2009.12.098.

(34) Berto, T. C.; Zhang, L.; Hamers, R. J.; Berry, J. F. Electrolyte Dependence of CO_2 Electroreduction: Tetraalkylammonium Ions Are Not Electrocatalysts. *ACS Catal.* **2015**, *5* (2), 703–707. https://doi.org/10.1021/cs501641z.

(35) Gambino, S.; Silvestri, G. On the Electrochemical Reduction of Carbon Dioxide and Ethylene. *Tetrahedron Lett.* **1973**, *14* (32), 3025–3028. https://doi.org/10.1016/S0040-4039(01)96310-5.

(36) Bordwell, F. G. Equilibrium Acidities in Dimethyl Sulfoxide Solution. *Acc. Chem. Res.* **1988**, *21* (12), 456–463. https://doi.org/10.1021/ar00156a004.

(37) Kolthoff, I. M.; Chantooni, M. K. Jr.; Bhowmik, S. Dissociation Constants of Uncharged and Monovalent Cation Acids in Dimethyl Sulfoxide. *J. Am. Chem. Soc.* **1968**, *90* (1), 23–28. https://doi.org/10.1021/ja01003a005.

(38) Olmstead, W. N.; Margolin, Z.; Bordwell, F. G. Acidities of Water and Simple Alcohols in Dimethyl Sulfoxide Solution. *J. Org. Chem.* **1980**, *45* (16), 3295–3299. https://doi.org/10.1021/jo01304a032.

(39) Staroverov, V. N.; Scuseria, G. E.; Tao, J.; Perdew, J. P. Comparative Assessment of a New Nonempirical Density Functional: Molecules and Hydrogen-Bonded Complexes. *J. Chem. Phys.* **2003**, *119* (23), 12129–12137. https://doi.org/10.1063/1.1626543.

(40) Tao, J.; Perdew, J. P.; Staroverov, V. N.; Scuseria, G. E. Climbing the Density Functional Ladder: Nonempirical Meta-Generalized Gradient Approximation Designed for Molecules and Solids. *Phys. Rev. Lett.* **2003**, *91* (14), 146401. https://doi.org/10.1103/PhysRevLett.91.146401.

(41) Xiao, W.; Zhang, J.; Wu, J. Recent Advances in Reactions Involving Carbon Dioxide Radical Anion. *ACS Catal.* **2023**, *13* (24), 15991–16011. https://doi.org/10.1021/acscatal.3c04125.

(42) Rodriguez, M. M.; Stubbert, B. D.; Scarborough, C. C.; Brennessel, W. W.; Bill, E.; Holland, P. L. Isolation and Characterization of Stable Iron(I) Sulfide Complexes. *Angew. Chem. Int. Ed.* **2012**, *51* (33), 8247–8250. https://doi.org/10.1002/anie.201202211.

(43) Bill, E. Iron-Sulfur Clusters—New Features in Enzymes and Synthetic Models. *Hyperfine Interactions* **2012**, *205* (1), 139–147. https://doi.org/10.1007/s10751-011-0411-8.

(44) DeRosha, D. E.; Chilkuri, V. G.; Van Stappen, C.; Bill, E.; Mercado, B. Q.; DeBeer, S.; Neese, F.; Holland, P. L. Planar Three-Coordinate Iron Sulfide in a Synthetic [4Fe-3S] Cluster with Biomimetic Reactivity. *Nat. Chem.* **2019**, *11* (11), 1019–1025. https://doi.org/10.1038/s41557-019-0341-7.

(45) Le, L. N. V.; Joyce, J. P.; Oyala, P. H.; DeBeer, S.; Agapie, T. Highly Activated Terminal Carbon Monoxide Ligand in an Iron–Sulfur Cluster Model of FeMco with Intermediate Local Spin State at Fe. *J. Am. Chem. Soc.* **2024**, *146* (8), 5045–5050. https://doi.org/10.1021/jacs.3c12025.

(46) Spiller, N.; Bjornsson, R.; DeBeer, S.; Neese, F. Carbon Monoxide Binding to the Iron–Molybdenum Cofactor of Nitrogenase: A Detailed Quantum Mechanics/Molecular Mechanics Investigation. *Inorg. Chem.* **2021**, *60* (23), 18031–18047. https://doi.org/10.1021/acs.inorgchem.1c02649.

(47) Osiewacz, J.; Löffelholz, M.; Weseler, L.; Turek, T. CO Poisoning of Silver Gas Diffusion Electrodes in Electrochemical CO_2 Reduction. *Electrochim. Acta* **2023**, *445*, 142046. https://doi.org/10.1016/j.electacta.2023.142046.

(48) Sun, M.-J.; Chen, M.; Si, D.-H.; Wu, Y.; Zhang, T.; Cao, R. Eliminating CO Poisoning in a Porous Metal–Organic Framework Catalyst for Highly Active Electrochemical CO_2 Reduction. *CCS Chem.* **2025**, *0* (0), 1–11. https://doi.org/10.31635/ccschem.025.202505666.

(49) Chen, X.; Granda-Marulanda, L. P.; McCrum, I. T.; Koper, M. T. M. How Palladium Inhibits CO Poisoning during Electrocatalytic Formic Acid Oxidation and Carbon Dioxide Reduction. *Nat. Commun.* **2022**, *13* (1), 38. https://doi.org/10.1038/s41467-021-27793-5.

(50) Guo, S.; Liu, Y.; Murphy, E.; Ly, A.; Xu, M.; Matanovic, I.; Pan, X.; Atanassov, P. Robust Palladium Hydride Catalyst

for Electrocatalytic Formate Formation with High CO Tolerance. *Appl. Catal. B: Environ.* **2022**, *316*, 121659. https://doi.org/10.1016/j.apcatb.2022.121659.
(51) Herrero, E.; Feliu, J. M. Understanding Formic Acid Oxidation Mechanism on Platinum Single Crystal Electrodes. *Curr. Opin. Electrochem.* **2018**, *9*, 145–150. https://doi.org/10.1016/j.coelec.2018.03.010.
(52) Wuttig, A.; Ryu, J.; Surendranath, Y. Electrolyte Competition Controls Surface Binding of CO Intermediates to CO_2 Reduction Catalysts. *J. Phys. Chem. C* **2021**, *125* (31), 17042–17050. https://doi.org/10.1021/acs.jpcc.1c04337.
(53) Rohde, M.; Laun, K.; Zebger, I.; Stripp, S. T.; Einsle, O. Two Ligand-Binding Sites in CO-Reducing V Nitrogenase Reveal a General Mechanistic Principle. *Sci. Adv.* **2021**, *7* (22), eabg4474. https://doi.org/10.1126/sciadv.abg4474.
(54) Buscagan, T. M.; Perez, K. A.; Maggiolo, A. O.; Rees, D. C.; Spatzal, T. Structural Characterization of Two CO Molecules Bound to the Nitrogenase Active Site. *Angew. Chem. Int. Ed.* **2021**, *60* (11), 5704–5707. https://doi.org/10.1002/anie.202015751.
(55) Gee, L. B.; Myers, W. K.; Nack-Lehman, P. A.; Scott, A. D.; Yan, L.; George, S. J.; Dong, W.; Dapper, C. H.; Newton, W. E.; Cramer, S. P. Nitrogenase Chemistry at 10 Kelvin—Phototautomerization and Recombination of CO-Inhibited α-H195Q Enzyme. *Inorg. Chem.* **2022**, *61* (30), 11509–11513. https://doi.org/10.1021/acs.inorgchem.2c00818.
(56) Chang, X.; Vijay, S.; Zhao, Y.; Oliveira, N. J.; Chan, K.; Xu, B. Understanding the Complementarities of Surface-Enhanced Infrared and Raman Spectroscopies in CO Adsorption and Electrochemical Reduction. *Nat. Commun.* **2022**, *13* (1), 2656. https://doi.org/10.1038/s41467-022-30262-2.
(57) France, J.; Hollins, P. Interactions of CO Molecules Adsorbed on Gold. *J. Electron Spectrosc. Relat. Phenom.* **1993**, *64–65*, 251–258. https://doi.org/10.1016/0368-2048(93)80086-2.
(58) Wuttig, A.; Yaguchi, M.; Motobayashi, K.; Osawa, M.; Surendranath, Y. Inhibited Proton Transfer Enhances Au-Catalyzed CO_2-to-Fuels Selectivity. *Proc. Natl. Acad. Sci. U.S.A.* **2016**, *113* (32), E4585–E4593. https://doi.org/10.1073/pnas.1602984113.
(59) Pavlishchuk, V. V.; Addison, A. W. Conversion Constants for Redox Potentials Measured versus Different Reference Electrodes in Acetonitrile Solutions at 25°C. *Inorg. Chim. Acta* **2000**, *298* (1), 97–102. https://doi.org/10.1016/S0020-1693(99)00407-7.
(60) Sengupta, K.; Joyce, J. P.; Decamps, L.; Kang, L.; Bjornsson, R.; Rüdiger, O.; DeBeer, S. Investigating the Molybdenum Nitrogenase Mechanistic Cycle Using Spectroelectrochemistry. *J. Am. Chem. Soc.* **2025**, *147* (2), 2099–2114. https://doi.org/10.1021/jacs.4c16047.
(61) Deniz, E.; Schmidt-Engler, J. M.; Ulrich, K.; Oberle, M.; Wille, G.; Bredenbeck, J. SH—It Happens: S–H Bonds as Intrinsic 2D-IR Labels in Proteins. *J. Chem. Phys.* **2022**, *157* (13), 135102. https://doi.org/10.1063/5.0107057.
(62) Tai, H.; Nishikawa, K.; Higuchi, Y.; Mao, Z.; Hirota, S. Cysteine SH and Glutamate COOH Contributions to [NiFe] Hydrogenase Proton Transfer Revealed by Highly Sensitive FTIR Spectroscopy. *Angew. Chem. Int. Ed.* **2019**, *58* (38), 13285–13290. https://doi.org/10.1002/anie.201904472.

Table of Contents artwork